Journal of Biomolecular NMR, **18:** 13–22, 2000.
KLUWER/ESCOM

Heteronuclear relayed E.COSY revisited: Determination of $^3J(H^\alpha,C^\gamma)$ couplings in Asx and aromatic residues in proteins

Frank Löhr[a], Carlos Pérez[a], Rolf Köhler[a], Heinz Rüterjans[a] & Jürgen M. Schmidt[b,*]
[a]*Institut für Biophysikalische Chemie, Johann Wolfgang Goethe-Universität, Biozentrum N230, Marie-Curie-Strasse 9, D-60439 Frankfurt am Main, Germany*
[b]*Division of Molecular Structure, National Institute for Medical Research, Mill Hill, London NW7 1AA, U.K.*

Received 20 April 2000; Accepted 9 June 2000

Key words: χ_1-angle, flavodoxin, multiple-quantum line-narrowing, multiplet simulation, ribonuclease T1, vicinal coupling constants

Abstract

Constant-time 3D heteronuclear relayed E.COSY [Schmidt et al. (1996) *J. Biomol. NMR*, **7**, 142–152], as based on generic 2D small-flip-angle HMQC-COSY [Schmidt et al. (1995) *J. Biomol. NMR*, **6**, 95–105], has been modified to allow for quantitative determination of heteronuclear three-bond $^3J(H^\alpha,C^\gamma)$ couplings. The method is applicable to amino acid spin topologies with carbons in the γ position which lack attached protons, i.e. to asparagine, aspartate, and aromatic residues in uniformly ^{13}C-enriched proteins. The pulse sequence critically exploits heteronuclear triple-quantum coherence (HTQC) of CH_2 moieties involving geminal H^β proton pairs, taking advantage of improved multiple-quantum relaxation properties, at the same time avoiding scalar couplings between those spins involved in multiple-quantum coherence, thus yielding E.COSY-type multiplets with a splitting structure that is simpler than with the original scheme. Numerical least-squares 2D line-shape simulation is used to extract $^3J(H^\alpha,C^\gamma)$ coupling constants which are of relevance to side-chain χ_1 dihedral-angle conformations in polypeptides. Methods are demonstrated with recombinant ^{15}N,^{13}C-enriched ribonuclease T1 and *Desulfovibrio vulgaris* flavodoxin with bound oxidized FMN.

Abbreviations: E.COSY, exclusive correlation spectroscopy; HMQC, heteronuclear multiple-quantum coherence; HTQC, heteronuclear triple-quantum coherence.

Introduction

^3J coupling constants probe the orientation of bond vectors between pairs of nuclei and impose restrictions on torsion angles to aid the convergence of molecular structure calculations primarily based on distance constraints. Recent extensive studies on ^3J coupling constants related to the protein backbone torsion angle ϕ (Löhr and Rüterjans, 1995, 1999; Schmidt et al., 1996; Löhr et al., 1997; Blümel et al., 1998) yielded highly accurate self-consistent torsion-angle constraints (Schmidt et al., 1999) without any recourse to NOE-derived distance information. This encouraged comprehensive measurements of ^3J coupling constants to obtain constraints on polypeptide side-chain torsion angles $\chi_1(N–C^\alpha–C^\beta–C^\gamma)$ as well.

Two general approaches are nowadays adopted in determining scalar coupling constants:
(i) *Frequency-modulation schemes* comprising COSY, DQF-COSY, E.COSY, and related techniques (Aue et al., 1976; Piantini et al., 1982; Griesinger et al., 1986) give rise to split and/or shifted lines in multiplet fine structure from which to determine the *J*-coupling constant.
(ii) *Amplitude-modulation schemes* including quantitative *J*-correlation experiments (Bax et al., 1994) yield cross peaks lacking significant fine structure, coding information on the *J*-coupling constant in sig-

*To whom correspondence should be addressed. E-mail: j.schmidt@nimr.mrc.ac.uk

nal intensity instead. The advantage of amplitude over frequency modulation lies in its greater sensitivity and thus its applicability to larger molecules in solution. However, frequency modulation schemes are unrivalled when J coupling constants are significantly smaller than apparent linewidths, e.g., $\pi J < (3 \ldots 5T_2^*)^{-1}$.

Here, we report on the measurement of $^3J(H^\alpha,C^\gamma)$ coupling constants in amino acid spin topologies with an unprotonated C^γ carbon. Although quantitative J-correlation studies have been carried out by Vuister and Bax (1993) on $^3J(H^\alpha,C^\gamma)$ coupling constants involving γ-methyl carbons, useful methods for investigating aspartate, asparagine, and aromatic residues have not been developed as yet. This prompted us to revisit E.COSY-based concepts, of which heteronuclear relayed E.COSY is an example which has proved successful in determining a variety of coupling constants in peptides (Schmidt et al., 1995) as well as proteins (Schmidt et al., 1996). The original scheme has been modified here in order to exploit heteronuclear triple-quantum coherence (HTQC) in methylene groups (Schmidt and Rüterjans, 1990), henceforth termed HTQC-COSY.

Methods

Basic E.COSY relies on a three-spin/three-coupling topology in which the active coupling between two spins produces a 2D correlation multiplet, while the other two passive couplings to the third spin show up as modulations in the multiplet fine structure (Griesinger et al., 1986). A characteristic tilt observed in the 2D multiplet pattern, eventually yielding the target coupling constant, arises from resonance-frequency differences between the pair of principal E.COSY signal constituents associated with $|\alpha\rangle$ and $|\beta\rangle$ states of the passive spin. Heteronuclear relayed E.COSY, also known as small-flip-angle HMQC-COSY (Schmidt et al., 1995), takes advantage of an additional auxiliary spin to mediate magnetization transfer between the active spins. This concept of relayed E.COSY can be extended to a pair of auxiliary spins, both in order to achieve faster magnetization transfer and to avoid unnecessary multiplet splittings. Suitable relay spins are the geminal protons in a CH_2 group. It should be noted that the presence of the $^2J_{HH}$ coupling would attenuate the signal rather than induce multiplet line splittings in constant-time versions of HMQC-COSY spectra based on CH double-quantum coherence (Schmidt et al., 1996). Leaving aside relaxation issues, this is the major argument in favour of the triple-quantum edited scheme, the pulse sequence of which is depicted in Figure 1. It suffices here to highlight the features particular to the 3D ct-HTQC-COSY, as the basic response calculations for the 2D small-flip-angle and 3D ct-HMQC-COSY pulse sequences have been presented previously (Schmidt et al., 1995, 1996) and the spin nomenclature employed is that used in those references.

Given a cyclic five-spin coupling topology -I_2-(I_1I_1)-S_1-S_2- with I and S denoting proton and – in the present case – carbon spins, respectively, the fragment $I_1I_1S_1$ is subject to heteronuclear triple-quantum coherence excitation (Schmidt and Rüterjans, 1990). Chemical shifts of the active spins S_1 and I_2 determine the location of the E.COSY-type multiplet at the coordinates $(\omega_{S_1}, \omega_{I_2})$ in a 2D spectrum, while S_2 is identified with the passive spin whose interaction with I_2, i.e. the coupling constant $J_{I_2S_2}$, is the desired structure parameter. To measure the $^3J(H^\alpha,C^\gamma)$ coupling constant in a typical amino acid spin topology, spins I_2, $I_1^{(1)}$, $I_1^{(2)}$, S_1, and S_2 are identified with H^α, $H^{\beta2}$, $H^{\beta3}$, C^β, and C^γ, respectively, disregarding any stereospecific assignments. Auxiliary spins $I_1^{(1)}$ and $I_1^{(2)}$ are mutually exchangeable and share almost identical properties, so as to form a pseudo-spin entity denoted ($I_1^{(1)}I_1^{(2)}$), or in short, (I_1I_1).

Subject to the initial DEPT pulse cluster, equilibrium proton magnetization, $\sigma_0 = I_{1z}^{(1)} + I_{1z}^{(2)}$, is converted first into a mixture of heteronuclear zero- and double-quantum coherence, the product operators of which are

$$\begin{aligned}\sigma_1 \;=\; & 2S_{1y}\left(I_{1x}^{(1)} + I_{1x}^{(2)}\right)\sin(\pi J_{I_1S_1}\tau)\cos(\pi J_{I_1I_1}\tau) \\ & + 4S_{1y}\left(I_{1y}^{(1)}I_{1z}^{(2)} + I_{1z}^{(1)}I_{1y}^{(2)}\right) \\ & \sin(\pi J_{I_1S_1}\tau)\sin(\pi J_{I_1I_1}\tau) \qquad (1)\end{aligned}$$

and second, following the full duration 2τ totalling $(J_{I_1S_1})^{-1}$, into heteronuclear triple-quantum coherence

$$\begin{aligned}\sigma_2 \;&=\; 4S_{1x}\left(I_{1x}^{(1)}I_{1y}^{(2)} + I_{1y}^{(1)}I_{1x}^{(2)}\right) \\ &=\; 2S_{1x}\{2QC\}_y \qquad (2)\end{aligned}$$

where the anti-phase term in Equation 1 due to the evolving homonuclear geminal coupling cancels upon phase cycling later in the experiment, while attenuation of in-phase magnetization by the cosine factor is considered to be negligible for typical values of $^2J(H^{\beta2},H^{\beta3})$. Partial evolution of S_1-chemical shift and

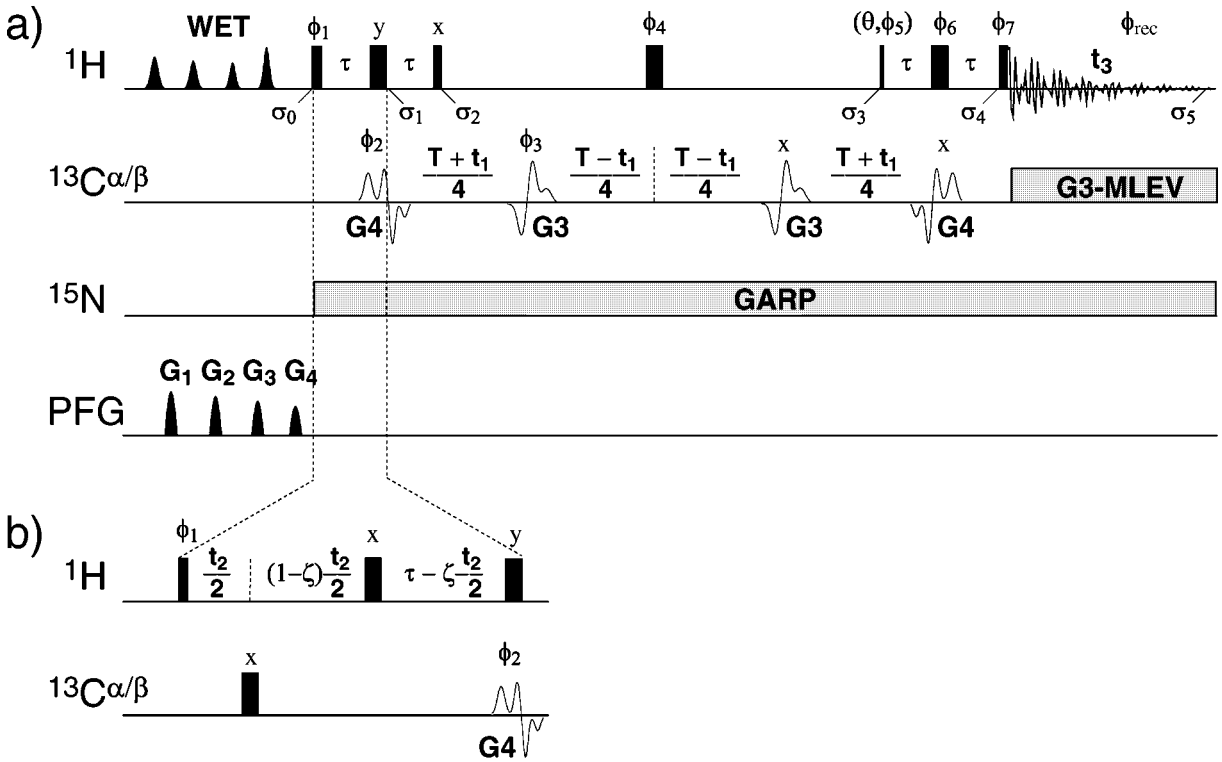

Figure 1. Pulse scheme of the constant time HTQC-COSY experiments for determining $^3J(H^{\alpha},C^{\gamma})$ coupling constants in Asx and aromatic amino acids in proteins; (a) 2D version and (b) 3D version. Narrow and wide vertical bars are $\pi/2$ and π pulses, respectively, while $\theta = 35°$ (see Methods). Critical durations were set at $\tau = 3.5$ ms and T = 29.4 ms to match $(2^1J_{CH})^{-1}$ and $(^1J_{C\alpha C\beta})^{-1}$, respectively. The residual HDO signal is suppressed by the WET sequence (Smallcombe et al., 1995) using magic-angle gradients (Mattiello et al., 1996) with the proton carrier frequency ω_0 set at the solvent resonance (4.68–4.72 ppm depending on sample protein and temperature). Gaussian cascades G4 and G3 (Emsley and Bodenhausen, 1990) with durations of 500 μs and 350 μs (600 MHz) or 500 μs and 300 μs (800 MHz), respectively, are used for selective excitation and refocusing of $^{13}C^{\alpha}$ and $^{13}C^{\beta}$ magnetization with the carbon carrier frequency set at 45 ppm. The second G4 pulse has a time-reversed shape. Band-selective $^{13}C^{\alpha}$ decoupling during acquisition is accomplished by an MLEV-16 expansion of 800-μs G3 pulses (Eggenberger et al., 1992) applied at 53 ppm. GARP-1 modulation (Shaka et al., 1985) with a nominal rf field strength of 0.78 kHz (600 MHz) or 0.96 kHz (800 MHz) is used for ^{15}N decoupling during all periods except the relaxation delay. Phase cycling is as follows: ϕ_1 = x; ϕ_2 = x, −x; ϕ_3 = 8(x), 8(y); ϕ_4 = x, −x; ϕ_5 = 2(x), 2(−x), 2(y), 2(−y); $\phi_6 = \phi_5 + \pi/2$; ϕ_7 = 4(y), 4(−x); ϕ_{rec} = x, 2(−x), x, −y, 2(y), −y, −x, 2(x), −x, y, 2(−y), y. Sign discrimination in F_1 and F_2 is achieved by States-TPPI (Marion et al., 1989) of ϕ_2 and ϕ_1, respectively. The t_2 dimension is of the semi-constant time variety (Logan et al., 1992; Grzesiek and Bax, 1993) with ζ set at 0.5 in the present application.

couplings involving I_2 have been ignored for reasons discussed later, and virtually identical coupling constants have been assumed for both $^1J(H^{\beta 2},C^{\beta})$ and $^1J(H^{\beta 3},C^{\beta})$. A convenient shorthand notation has been introduced for the proton double-quantum portion (Ernst et al., 1987).

Magnetization then propagates from the selected $I_1I_1S_1$ triple-quantum coherence to the target spin I_2. Coherence transfer in HTQC-COSY is in principle mediated through two simultaneous pathways being associated with *relayed* ($S_1 \rightarrow (I_1I_1) \rightarrow I_2$) and *direct* ($S_1 \rightarrow I_2$) interaction via the non-distinguishable homonuclear composite coupling $\Sigma J_{I_1I_2} = J_{I_1^{(1)}I_2} + J_{I_1^{(2)}I_2}$ and the usually small heteronuclear coupling $J_{S_1I_2}$, respectively. However, the three symmetrically arranged 180° pulses applied to ^{1}H and ^{13}C nuclei during the t_1 evolution period (Figure 1a) perfectly refocus the effect of the *direct* coupling $J_{S_1I_2}$, leaving only the *relay* contribution relevant in HTQC-COSY, unlike its predecessor (Schmidt et al., 1996). Terms not involving I_2 give rise to COSY-type dispersive auto-peaks which are not considered further. Given the effective magnetization-transfer period $T_c = T - 2\tau$, the only relevant term anti-phase with respect to I_2 at

the end of t_1 and t_2 in a 3D application (Figure 1b) is

$$\begin{aligned}\sigma_3 &= -8S_{1x}\left(I_{1x}^{(1)}I_{1x}^{(2)} - I_{1y}^{(1)}I_{1y}^{(2)}\right) I_{2z} \\ &\quad \sin(\pi\Sigma J_{I_1I_2}T_c)\cos(\omega_{I_1t_2})\cos(\omega_{S_1t_1}) \\ &= -8S_{1x}\{2QC\}_x I_{2z}\sin(\pi\Sigma J_{I_1I_2}T_c) \\ &\quad \cos(\omega_{I_1t_2})\cos(\omega_{S_1t_1}) \qquad (3)\end{aligned}$$

where the effect of the refocusing π pulses has been incorporated. The transfer intensity is dominated by the T_c-dependent term representing a mere scaling in constant-time experiments. The second DEPT pulse cluster includes the small-flip-angle pulse θ set at 35° to maximize the transfer $\{2QC\}_x I_{2z} \rightarrow (I_{1z}^{(1)}I_{1y}^{(2)} - I_{1y}^{(1)}I_{1z}^{(2)})I_{2z}$, restoring during the first period τ the heteronuclear I_1S_1 double-antiphase magnetization with respect to I_2, which refocuses during the final period τ under either coupling $J_{I_1S_1}$ to yield the relevant terms

$$\begin{aligned}\sigma_4 &= 2\left(I_{1x}^{(1)} + I_{1x}^{(2)}\right) I_{2z}\sin\theta\cos^2\theta \\ &\quad \sin(\pi\Sigma J_{I_1I_2}T_c)\cos(\omega_{I_1t_2})\cos(\omega_{S_1t_1}) \qquad (4)\end{aligned}$$

The small-flip-angle ^{1}H pulse θ is not of the usual E.COSY type, its merits being the optimal conversion of proton multiple-quantum into double-antiphase terms. The final proton COSY-type mixing pulse transfers polarization onto the I_2 spin evolving into observable magnetization according to

$$\begin{aligned}\sigma_5 &= I_{2y}\sin\theta\cos^2\theta\sin(\pi\Sigma J_{I_1I_2}T_c) \\ &\quad \sin(\pi\Sigma J_{I_1I_2}t_3)\sin(\omega_{I_2}t_3)\cos(\omega_{I_1t_2}) \\ &\quad \cos(\omega_{S_1t_1}) \qquad (5)\end{aligned}$$

This is the basic correlation signal located at $(\omega_{S_1}, \omega_{I_1}, \omega_{I_2})$ in a 3D spectrum as arising from the relayed coherence-transfer pathway. Chemical shifts in t_1 and t_3 associated with spins S_1 and I_2, respectively, span the dimensions of a 2D subspectrum, while advantage is taken from I_1 precession spreading congested regions of the spectrum into a third dimension. In contrast with previous schemes, no line splittings appear due to active $J_{I_1I_2}$ and $J_{S_1I_2}$ or passive $J_{I_1I_1}$ couplings along the indirect dimension ω_1 as a consequence of multiple-quantum shift evolution and the symmetric pulse-sequence design. Multiplet splitting properties in the acquisition dimension ω_3 are dominated by an antiphase doublet with respect to the active homonuclear composite coupling $\Sigma J_{I_1I_2}$.

The 3D relayed E.COSY-type multiplet structure is fully appreciated only when the remote spin S_2 passively coupled to all of the three active spins S_1, I_2, and $I_1^{(1)}$ or $I_1^{(2)}$, depending on the 3D multiplet considered, is introduced. A combination of unique S_2 chemical-shift ranges in the downfield spectral region and selective excitation techniques ensures that the $|\alpha\rangle$ and $|\beta\rangle$ states of the S_2 spin are conserved during the experiment. Effects are described by expanding Equation 5 using polarization operators, $S_2^{\alpha} = 1/2 + S_{2z}$ and $S_2^{\beta} = 1/2 - S_{2z}$, and composite frequencies, $\Sigma_1 = \omega_{S_1} + \pi J_{S_1S_2}$, $\Delta_1 = \omega_{S_1} - \pi J_{S_1S_2}$, $\Sigma_2 = \omega_{I_1} + \pi J_{I_1S_2}$, $\Delta_2 = \omega_{I_1} - \pi J_{I_1S_2}$, $\Sigma_3 = \omega_{I_2} + \pi J_{I_2S_2}$, $\Delta_3 = \omega_{I_2} - \pi J_{I_2S_2}$, as follows:

$$\begin{aligned}\sigma_5' = -I_{2y}\sin\theta\cos^2\theta\sin(\pi\Sigma J_{I_1I_2}T_c)\sin(\pi\Sigma J_{I_1I_2}t_3) \\ \times\left\{S_2^{\alpha}\cos(\Sigma_3t_3) + S_2^{\beta}\cos(\Delta_3t_3)\right\} \\ \times\left\{S_2^{\alpha}\cos(\Sigma_2t_2) + S_2^{\beta}\cos(\Delta_2t_2)\right\} \\ \times\left\{S_2^{\alpha}\cos(\Sigma_1t_1) + S_2^{\beta}\cos(\Delta_1t_1)\right\} \qquad (6)\end{aligned}$$

The observable terms, $I_{2y}S_2^{\alpha}$ and $I_{2y}S_2^{\beta}$, give rise to a 3D E.COSY multiplet with principal components located at positions $(\Sigma_1,\Sigma_2,\Sigma_3)$ and $(\Delta_1,\Delta_2,\Delta_3)$, respectively. The sought coupling constant is taken from the displacement along ω_3, i.e. $J_{I_2S_2} = (\Sigma_3 - \Delta_3)/2\pi$.

Experimental

Heteronuclear triple-quantum relayed E.COSY experiments were carried out on Bruker DMX-600 and DRX-800 spectrometers equipped with 5-mm triple-resonance probes and three-axis pulsed-field gradient (PFG) accessories. Details of the pulse-sequence setup are given in the legend to Figure 1. Sample molecules used were two proteins for which fairly precise X-ray structures are available, the 104-amino acid ribonuclease T1 (Martinez-Oyanedel et al., 1991) and the 147-amino acid oxidized *Desulfovibrio vulgaris* flavodoxin (Watt et al., 1991). Details of spectrum processing procedures are included in the legends to Figures 2 and 3.

Determination of the coupling constant $^3J(H^{\alpha},C^{\gamma})$ in amino-acid spin topologies comprising H^{α}, ($H^{\beta 2}$, $H^{\beta 3}$), C^{β}, and C^{γ}, exploits large $^1J(C^{\beta},C^{\gamma})$ couplings of 35–50 Hz to separate the two principal E.COSY multiplet components. Multiplets in 3D spectra are located at $(\Omega_{C^{\beta}}, \Omega_{H^{\beta 2}}, \Omega_{H^{\alpha}})$ and $(\Omega_{C^{\beta}}, \Omega_{H^{\beta 3}}, \Omega_{H^{\alpha}})$. A small number of t_2 increments provide adequate resolution in the ω_2 dimension of H^{β}-chemical shifts. Heteronuclear couplings such as $^2J(H^{\beta},C^{\gamma})$ are not resolved in the ω_2 dimension, as they are usually smaller

than both the F_2-digital resolution and the linewidth. This allows two-dimensional (ω_1,ω_3) projections to be readily computed for quantitative 2D lineshape analysis.

The multiple-parameter fit applied to extract $^3J(H^\alpha,C^\gamma)$ coupling constants from the E.COSY-type experimental multiplet patterns employed 2D matrices of 32×32 or 32×64 data points, each being centered at the approximate (ω_1,ω_3) chemical-shift coordinates of the selected signal. Simulated multiplet patterns were obtained by projection-multiplication methods as previously described (Schmidt et al., 1996), basically using those routines with the fit parameter corresponding to the direct coupling pathway $^2J(H^\alpha,C^\beta)$ constrained at zero and the value of the delay τ negated to reflect the altered timings introduced by the DEPT pulse clusters. The model function of the two-dimensional (C^β,H^α) multiplet, parametrized into the control variables as summarized in Table 1, is given by

$$\begin{aligned}\sigma_{obs} \;=\; & I_{y,H^\alpha}\cos^2(\pi t_1/2t_1^{max})\sin(\pi t_3/2t_3^{max}) \\ & \sin(\pi\Sigma J_{H^\alpha H^\beta}t_3) \\ & \times\exp(-\pi R_{C^\beta}t_1)\left\{S^\alpha_{C^\gamma}\cos(\Sigma_1 t_1)\right. \\ & \qquad\left. + S^\beta_{C^\gamma}\cos(\Delta_1 t_1)\right\} \\ & \times\exp(-\pi R_{H^\alpha}t_3)\left\{S^\alpha_{C^\gamma}\cos(\Sigma_3 t_3)\right. \\ & \qquad\left. + S^\beta_{C^\gamma}\cos(\Delta_3 t_3)\right\} \end{aligned} \tag{7}$$

which emerged from Equation 6 having eliminated t_2 and provided the constant duration $T_c = (T - 2\tau) = (J_{C^\alpha C^\beta})^{-1} - (J_{H^\beta C^\beta})^{-1}$. The model includes relaxation and apodization effects, where sum and difference symbols denote composite frequencies $\Sigma_1 = \Omega_{C^\beta} + \pi J_{C^\beta C^\gamma}$, $\Delta_1 = \Omega_{C^\beta} - \pi J_{C^\beta C^\gamma}$, $\Sigma_3 = \Omega_{H^\alpha} + \pi J_{H^\alpha C^\gamma}$, and $\Delta_3 = \Omega_{H^\alpha} - \pi J_{H^\alpha C^\gamma}$. The line-broadening parameter associated with t_1 mainly accounted for B_0-field inhomogeneity effects under constant-time evolution. Based on the identity $\sin(\pi\Sigma J_{H^\alpha H^\beta}t) = \sin(\pi J_{H^\alpha H^{\beta 2}}t)\cos(\pi J_{H^\alpha H^{\beta 3}}t) + \cos(\pi J_{H^\alpha H^{\beta 2}}t)\sin(\pi J_{H^\alpha H^{\beta 3}}t)$, the non-distinguishable composite transfer coupling $\Sigma J_{H^\alpha H^\beta} = J_{H^\alpha H^{\beta 2}} + J_{H^\alpha H^{\beta 3}}$ was fitted as a single parameter, while avoiding additional modulations with respect to $^2J(H^{\beta 2},H^{\beta 3})$ as a consequence of CH_2 triple-quantum states involving both H^β relay spins in a pseudo-spin fashion. In practice, it was found necessary to expand the model by an additional pair of E.COSY splittings due mainly to the presence of two backbone carbonyl carbons C'_i and C'_{i-1} of the current and preceding residue, respectively. However, the couplings incurred, $^2J(H^\alpha_i,C'_i)$, $^2J(C^\beta_i,C'_i)$, $^3J(H^\alpha_i,C'_{i-1})$, $^3J(C^\beta_i,C'_{i-1})$, cannot be assigned to particular carbons. Inclusion of additional long-range coupling parameters related to t_1 and t_3, e.g. $^2J(C^\beta,C^\delta)$ in aromatic side chains and any residual $^3J(H^\alpha,H^N)$ after deuterium exchange, respectively, was found to improve the fit not significantly. Details of the least-squares optimization protocol have been given previously (Schmidt et al., 1996; Schmidt, 1997).

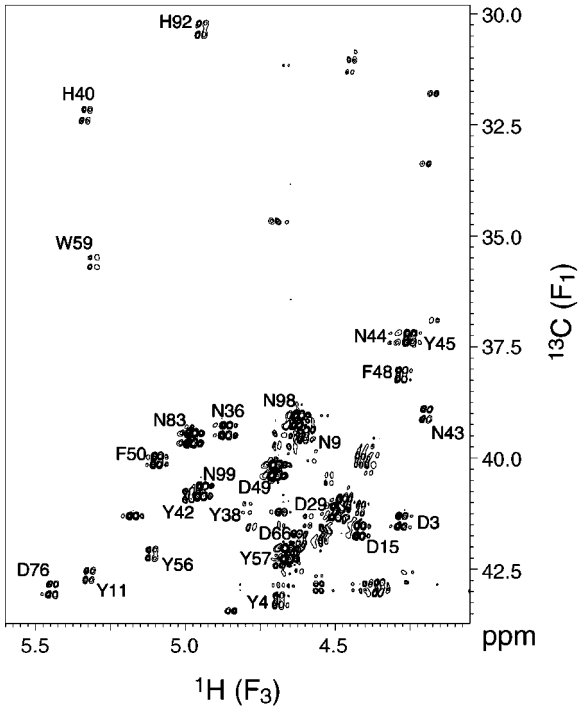

Figure 2. Excerpt from the 2D-constant time HTQC-COSY spectrum of $^{15}N,^{13}C$-labelled RNase T1 (2.5 mM in D_2O solution) recorded at 800 MHz and 308 K with the pulse sequence of Figure 1a. A total of 324 (t_1) × 480 (t_3) complex data points were sampled, corresponding to acquisition times of 28.4 ms and 82.2 ms, respectively, accumulating 32 transients per FID giving a total experiment time of 8 h. Time domain data in t_1 were doubled using linear prediction. Apodization involved multiplication with squared-cosine and sine window functions in t_1 and t_3, respectively. The 2D matrix was Fourier transformed to 2K × 2K real points to yield spectral resolutions of 5.55 and 2.85 Hz, covering total spectral widths of 11364 and 5841 Hz in the F_1 and F_3 dimensions, respectively. Positive and negative intensities are represented by dense and sparse contours, respectively. The (C^β,H^α) multiplets of aromatic and Asx residues in the chemical-shift range shown typically exhibit in-phase and anti-phase splittings and tilts are due to passive E.COSY couplings $^1J(C^\beta,C^\gamma)$ and $^3J(H^\alpha,C^\gamma)$ along F_1 and F_3, respectively.

Table 1. Fit parameters used in simulations of ct-HTQC-COSY (C^{β},H^{α}) multiplets[a]

Parameter type	Dimension	Association	Initial value
Intensity	n/a	A	rms
Apparent line width	F_1	R(C^{β})	2 Hz
Apparent line width	F_3	R(H^{α})	15 Hz
Position	F_1	$\Omega(C^{\beta})$	c.g.c.
Position	F_3	$\Omega(H^{\alpha})$	c.g.c.
Relayed-transfer couplings	F_3	$^3J(H^{\alpha},H^{\beta 2}) + {}^3J(H^{\alpha},H^{\beta 3})$	17 Hz
E.COSY splitting	F_1	$^1J(C^{\beta},C^{\gamma})$	48 Hz
E.COSY splitting	F_3	$^3J(H^{\alpha},C^{\gamma})$	2 Hz
E.COSY splitting(s)	F_1	$^2J(C^{\beta},C'_i) + {}^3J(C^{\beta},C'_{i-1})$	4 Hz
E.COSY splitting(s)	F_3	$^2J(H^{\alpha},C'_i) + {}^3J(H^{\alpha},C'_{i-1})$	1 Hz

[a] Amplitude and linewidth parameters are fitted in base-10 and natural logarithm, respectively, to avoid the need of constraining values to positive numbers. The initial amplitude derives from the root-mean-square (rms) intensity of the experimental multiplet. Positional parameters refer to the center coordinates of the selected multiplet submatrix, initialized at the center-of-gravity coordinates (c.g.c.) of the experimental multiplet.

Results and discussion

The pulse sequences for heteronuclear triple-quantum correlation (Schmidt and Rüterjans, 1990) and heteronuclear relayed E.COSY (Schmidt et al., 1995, 1996) have been merged to yield a novel correlation experiment for determining three-bond coupling constants in molecular fragments of the type Y-XH_2-X′H. Nuclei X and Y must be of different species, as is the case with carbon and nitrogen, or they must be capable of being excited separately using, for example, selective pulses. The choice for X′ is less restricted. Such a spin topology is present in a number of amino acid side chains containing the C^{γ}–$C^{\beta}H_2$–C^{α}H fragment, allowing access to the $^3J(H^{\alpha},C^{\gamma})$ coupling relevant to the conformation of the side-chain torsion χ_1. The experiment is restricted, however to aromatic and Asx residues as only these provide sufficient discrimination of C^{β} and C^{γ} carbon chemical-shift ranges, and it works for carbons in the γ position which lack attached hydrogens. Making use of the fragment C′–$C^{\alpha}H_2$–NH, 3D ct-HTQC-COSY is also expected to complement 3D ct-HMQC-COSY in that ϕ-related $^3J(H^N,C')$ coupling constants in glycine residues can be readily determined, not otherwise accomplished with the basic scheme.

The 2D version of the pulse scheme of Figure 1a was tested on ^{15}N,^{13}C-labelled RNase T1 an overview spectrum of which is shown in Figure 2. The 3D pulse scheme of Figure 1b was then applied to both RNase T1 and *D. vulgaris* flavodoxin. Numerical two-dimensional (C^{β},H^{α}) multiplet simulations, using previously established methods (Schmidt et al., 1996), were used to extract the sizeable $^1J(C^{\beta},C^{\gamma})$ and $^3J(H^{\alpha},C^{\gamma})$ values, from the F_1 and F_3 dimensions respectively, of the E.COSY-type multiplet. Simulations were marginally improved by the inclusion of further, unresolved, E.COSY-type splittings, presumably arising from interactions with backbone carbonyl atoms via $^2J(C_i^{\beta},C'_i)$ and $^2J(H_i^{\alpha},C'_i)$, and/or $^3J(C_i^{\beta},C'_{i-1})$ and $^3J(H_i^{\alpha},C'_{i-1})$. The presence of long-range interactions like $^2J(C^{\beta},C^{\delta})$ might attenuate signals of aromatic side chains with respect to those of Asn and Asp residues. In contrast to the earlier approach, COSY-type in-phase splittings involving other passive proton spins apart from those mentioned can be ignored, firstly because the protein was dissolved in D_2O, thus effectively removing the amide proton as an interaction partner, and secondly because hydrogens attached to C^{γ} were absent in the investigated spin systems.

$^3J(H^{\alpha},C^{\gamma})$ coupling constants in RNase T1 and *D. vulgaris* flavodoxin range from near 0 up to almost 10 Hz, in overall agreement with χ_1 rotamer states taken from the protein X-ray coordinate sets 9RNT (Martinez-Oyanedel et al., 1991) and 2FX2 (Watt et al., 1991), respectively (Figure 4). A few experimental values look incompatible with the theoretical χ_1-dihedral angle dependence of the $^3J(H^{\alpha},C^{\gamma})$ coupling constant, also shown in Figure 4, which, we emphasize, is tentative only. Proper Karplus parametrization of the $^3J(H^{\alpha},C^{\gamma})$ coupling deserves more detailed investigation beyond the scope of this paper. More likely, reasons of conflicting data are variation of $^3J(H^{\alpha},C^{\gamma})$ with amino acid topology, incompatibili-

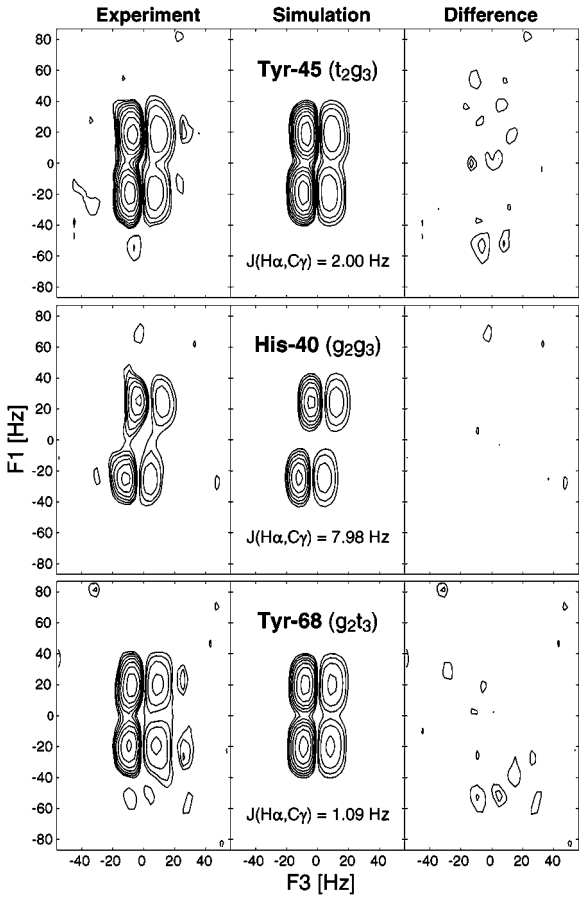

Figure 3. Representative (ω_1, ω_3) projections of (C^β,H^α) multiplets obtained from ^{15}N,^{13}C-labelled RNase T1 at 600 MHz and 308 K using the 3D ct-HTQC-COSY pulse sequence of Figure 1b. The 3D data set was recorded with acquisition times of 29.3, 14.1, and 89.2 ms collecting 164 × 18 × 320 complex points in the t_1, t_2, and t_3 dimensions, respectively, giving a total experiment time of 66 h. Following linear prediction of t_1 and t_2 data to 328 and 32 points, the 3D matrix was Fourier transformed to 1K × 64 × 1K real points to yield spectral resolutions of 5.43, 18.78, and 3.51 Hz, covering total spectral widths of 5556, 1202, and 3592 Hz in the F_1, F_2, and F_3 dimensions, respectively. Squared-cosine functions were used for apodization in the t_1 and t_2 dimensions, and a sinebell in t_3. Pure absorptive parts of the (C^β,H^α) multiplets displayed are two-dimensional (ω_1,ω_3) projections calculated by summing over appropriate ω_2 slices such as to include both multiplets at $H^{\beta 2}$ and $H^{\beta 3}$ frequencies in the ω_2 dimension. Positive and negative contours are drawn with level spacings of $\sqrt{2}$ and 2, respectively, with the lowest level at three times the rms noise intensity. Quantitative evaluation of the $^3J(H^\alpha,C^\gamma)$ coupling constants, values of which are indicated, was achieved by iterative multiplet simulation (Schmidt et al., 1996).

ties between NMR and X-ray structure, and perhaps molecular mobility. Panels in Figure 3 show multiplets typical of the three staggered rotamers encountered in amino acid side chains. Our results corroborate earlier investigations of $^3J(H^\alpha,H^\beta)$, $^3J(N,H^\beta)$, and $^3J(C',H^\beta)$ coupling constants (Karimi-Nejad, 1994), according to which Tyr-45, located in the nucleotide binding site of RNase T1, is likely to exhibit $\chi_1 \approx -60°$, in contrast with X-ray data hinting at $\chi_1 \approx +60°$(Martinez-Oyanedel et al., 1991). $\chi_1 \approx +60°$rotamers would give rise to large $^3J(H^\alpha,C^\gamma)$ couplings, as observed for His-40 located in the catalytic site of RNase T1, and to multiplets attenuated in intensity as both homonuclear transfer couplings are small. The unique $^3J(H^\alpha,C^\gamma)$ coupling helps discriminate side-chain rotamers in cases where the resonances of diastereotopic H^β protons are degenerate, as shown for Tyr-68 which adopts a $\chi_1 \approx \pm 180°$conformation. Results for $^3J(H^\alpha,C^\gamma)$ coupling parameters in RNase T1 are summarized in Table 2, while data for *D. vulgaris* flavodoxin will be included in a forthcoming study on amino acid side chain conformations in that protein.

Values of one-bond $^1J(C^\beta,C^\gamma)$ coupling constants were found to correlate with residue type, too, although these are not important to constrain dihedral-angle conformation. Averages and standard deviations (sample sizes in parentheses) compiled from both proteins are 45.5 ± 1.6 (11) and 49.5 ± 1.4 (23) for Asn and Asp residues, respectively. Mean values in aromatic side chains Tyr, Phe, Trp, and His are 40.9 ± 3.8 (14), 42.2 ± 2.7 (10), 46.6 ± 1.6 (3) and 47.9 ± 1.8 (4).

Depending on signal-to-noise (S/N), standard deviations of the five *J*-coupling fit parameters are ±0.45 Hz on average, normally considered minimum estimates as standard error-propagation methods exclusively reflect the statistical random error, ignoring non-linear parameter cross-correlation intrinsic to the model function. In multivariate optimization of the present multiplet models, covariance matrices typically break down into three parameter groups: (i) amplitude and linewidths; (ii) multiplet positions; and (iii) all the *J*-splitting parameters. Multiplet positions generally showed negligible cross-correlation with other fit parameters, exhibiting uncertainties of 0.9 and 0.4 Hz in F_1 and F_3, respectively. Standard deviations of linewidth parameters were typically 33% and 6% in F_1 and F_3, respectively, reflecting the higher spectral resolution in the acquisition dimension. To account for such parameter cross-correlation effects, confidence intervals of the *J*-coupling parame-

Table 2. J coupling constants in RNase T1 as determined from 3D-heteronuclear relayed E.COSY (600 MHz 3D HTQC-COSY)[a]

Residue	$\chi_{1,X-ray}$ (deg)	Primary E.COSY		Secondary E.COSY		Transfer couplings	Linewidths	
		$^3J(H^\alpha,C^\gamma)$ (Hz)	$^1J(C^\beta,C^\gamma)$ (Hz)	$\Sigma J(H^\alpha,C')$ (Hz)	$\Sigma J(C^\beta,C')$ (Hz)	$\Sigma J(H^\alpha,H^\beta)$ (Hz)	$\nu(H^\alpha)$ (Hz)	$\nu(C^\beta)$ (Hz)
Asn9	−67.9	0.4 ± 1.2	43.0 ± 2.7	0.9 ± 1.8	11.5 ± 2.0	17.3 ± 1.4	11.9	3.7
Asn36	−73.6	3.6 ± 0.4	46.3 ± 0.8	-0.6 ± 0.6	12.0 ± 0.5	16.6 ± 0.5	18.1	3.5
Asn43	−68.3	2.9 ± 0.4	45.7 ± 0.7	2.4 ± 0.5	10.5 ± 0.5	16.7 ± 0.4	16.2	2.2
Asn44	−166.7	3.6 ± 2.0	47.5 ± 3.8	1.8 ± 2.8	12.0 ± 2.6	27.3 ± 1.7	17.2	3.8
Asn81	+79.2	7.5 ± 2.2	43.3 ± 5.8	7.1 ± 1.5	-1.3 ± 4.7	18.7 ± 3.4	0.8	11.3
Asn83	−63.1	3.0 ± 0.3	46.1 ± 0.7	0.8 ± 0.4	11.9 ± 0.4	16.5 ± 0.4	17.4	2.9
Asn84	−163.8	6.7 ± 1.9	45.5 ± 3.9	10.1 ± 1.0	-3.1 ± 3.1	10.7 ± 0.9	17.2	12.9
Asn98	+28.3	3.4 ± 0.4	46.5 ± 0.8	1.0 ± 0.6	11.5 ± 0.6	17.3 ± 0.5	17.5	3.2
Asn99	−58.6	4.3 ± 0.3	44.3 ± 0.7	-0.7 ± 0.5	12.2 ± 0.5	16.3 ± 0.4	15.5	4.7
Asp3	−69.0	3.0 ± 0.4	49.4 ± 0.7	1.2 ± 0.5	12.0 ± 0.4	17.4 ± 0.5	18.5	1.0
Asp15	−68.4	1.9 ± 0.3	47.8 ± 0.6	0.7 ± 0.4	11.9 ± 0.4	16.8 ± 0.4	16.2	3.5
Asp29	−70.6	5.8 ± 0.9	48.9 ± 1.9	-0.4 ± 1.4	11.4 ± 1.6	17.1 ± 1.1	15.4	0.0
Asp49	−175.9	2.5 ± 0.3	48.9 ± 0.7	0.6 ± 0.5	I2.0 ± 0.5	15.3 ± 0.4	16.5	5.1
Asp66	−68.0	3.5 ± 0.3	47.6 ± 0.9	1.3 ± 0.5	12.2 ± 0.6	14.1 ± 0.4	14.4	5.0
Asp76	−54.3	2.0 ± 0.7	49.7 ± 1.3	0.8 ± 0.8	12.0 ± 0.7	16.3 ± 0.8	20.7	0.0
His27	+176.1	-0.5 ± 1.0	49.4 ± 2.2	-0.8 ± 1.5	12.7 ± 1.6	17.5 ± 1.2	17.4	6.1
His40	+61.0	8.0 ± 0.4	49.0 ± 1.0	-0.1 ± 0.7	11.1 ± 0.8	16.4 ± 0.5	14.1	6.9
His92	−73.6	4.2 ± 0.4	45.4 ± 1.1	1.9 ± 0.7	13.3 ± 0.9	15.3 ± 0.5	17.0	10.8
Phe48	−58.0	2.6 ± 0.4	39.0 ± 0.9	0.1 ± 0.6	11.6 ± 0.6	17.6 ± 0.5	15.3	2.9
Phe50	−68.2	2.3 ± 0.5	38.1 ± 1.1	0.8 ± 0.8	11.9 ± 0.8	14.7 ± 0.5	19.7	3.7
Phe80	+53.8	8.4 ± 1.0	44.0 ± 2.3	1.2 ± 1.3	11.7 ± 1.4	16.4 ± 1.2	12.4	1.7
Phe100	−68.2	3.7 ± 0.6	37.9 ± 1.3	1.9 ± 1.0	11.9 ± 1.0	17.0 ± 0.7	18.6	5.2
Trp59	+168.6	2.3 ± 0.9	44.8 ± 1.7	0.3 ± 1.5	10.6 ± 1.3	17.0 ± 1.1	20.1	3.4
Tyr4	−61.6	3.9 ± 1.1	41.7 ± 2.8	6.8 ± 1.2	2.0 ± 3.9	19.0 ± 1.8	6.9	12.4
Tyr11	−57.7	1.5 ± 0.6	38.5 ± 1.3	0.4 ± 0.9	12.0 ± 0.9	15.6 ± 0.7	17.4	5.1
Tyr24	−164.8	-0.3 ± 0.6	32.9 ± 1.1	-0.1 ± 0.9	12.7 ± 0.8	17.9 ± 0.7	17.5	4.3
Tyr38	−75.5	1.1 ± 1.2	40.8 ± 2.5	-0.6 ± 1.9	11.0 ± 1.9	16.3 ± 1.5	17.0	3.6
Tyr42	+169.7	1.8 ± 0.5	39.7 ± 1.1	1.4 ± 0.9	11.6 ± 0.9	15.2 ± 0.5	20.8	5.4
Tyr45	+63.2	2.0 ± 0.3	38.5 ± 0.6	-0.5 ± 0.4	12.5 ± 0.4	16.1 ± 0.3	17.4	4.8
Tyr56	−55.4	1.6 ± 0.6	35.2 ± 1.3	1.9 ± 0.9	12.5 ± 0.8	17.5 ± 0.8	16.5	3.0
Tyr57	−65.5	3.9 ± 1.1	44.1 ± 2.3	1.3 ± 1.6	11.5 ± 1.6	18.1 ± 1.4	14.4	2.9
Tyr68	−177.0	1.1 ± 0.4	40.5 ± 0.9	0.4 ± 0.6	12.4 ± 0.6	17.5 ± 0.5	16.8	4.8

[a]Best-fit parameters obtained with 2D lineshape simulation of (C^β,H^β,H^α) multiplets projected along F_2 with downfield and upfield H^β planes superimposed, unless degenerate. Residue names in italics indicate weak patterns with S/N < 10, producing wider confidence intervals in F-statistics (see text). Non-distinguishable composite couplings are: $\Sigma J(H^\alpha,H^\beta) = {}^3J(H^\alpha,H^{\beta 2}) + {}^3J(H^\alpha,H^{\beta 3})$; $\Sigma J(C^\beta,C') = {}^2J(C^\beta,C'_i) + {}^3J(C^\beta,C'_{i-1})$; $\Sigma J(H^\alpha,C') = {}^2J(H^\alpha,C'_i) + {}^3J(H^\alpha,C'_{i-1})$. Both latter variables may include further non-resolved splittings, e.g. due to carbon atoms in the side chain of aromatic residues (see text). X-ray reference data are calculated from PDB coordinates 9RNT (Martinez-Oyanedel et al.,1991).

ters have therefore been obtained from the analysis of variances (ANOVA) in the framework of F-statistics, as described elsewhere (Schmidt et al., 1996; Schmidt, 1997), and are supplied with J-coupling parameters in Table 2.

Variations in HTQC-COSY signal intensities arise to some degree from the range of values of the transfer couplings and from differing relaxation efficiencies of the H^α spin. Linewidths of typically 10–20 Hz emerged from the multiplet simulations. An extensive literature (Griffey and Redfield, 1987; Seip et al., 1992; Grzesiek and Bax, 1995; Swapna et al., 1997; Tessari et al., 1997; Sklenár et al., 1998; Gschwind et al., 1998) states that nuclear spin polarization in

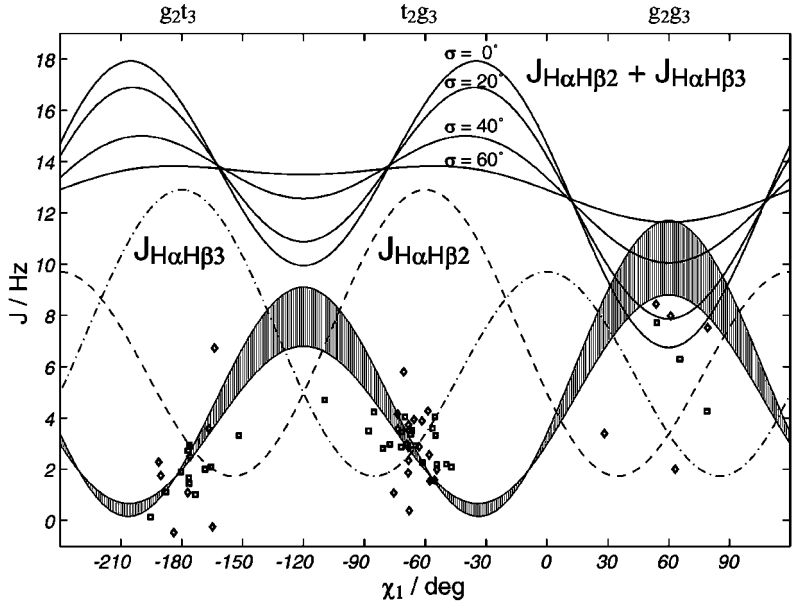

Figure 4. Experimental $^3J(H^\alpha,C^\gamma)$ coupling constants plotted against χ_1 values taken from RNase T1 (diamonds) and *D. vulgaris* flavodoxin (squares) X-ray coordinates of 9RNT (Martinez-Oyanedel et al., 1991) and 2FX2 (Watt et al., 1991) resolved at 1.5 Å and 1.9 Å, respectively. The tentative conformational dependence of $^3J(H^\alpha,C^\gamma)$ coupling constants on the dihedral angle χ_1 in proteins (hatched area) is bounded by Karplus curves given by Wasylishen and Schaefer (1972), $A = 7.1$, $B = -1.0$, $C = 0.7$ Hz, on the basis of ab initio calculations on propane and by DeMarco and Llinás (1979), $A = 10.2$, $B = -1.3$, $C = 0.2$ Hz, as derived from χ_2-related C^α–C^β–C^γ–H^γ fragments in ornithine residues. However, molecular templates used in these studies may not be suitable as substituent patterns do not match the H^α–C^α–C^β–C^γ fragments of Asx and aromatic residues. Magnetization transfer in HTQC-COSY in amino acid spin topologies depends on $^3J(H^\alpha,H^\beta)$ couplings as displayed using Karplus parameters $A = 9.5$, $B = -1.6$, $C = 1.8$ Hz (DeMarco et al., 1978). The composite J_{HH} coupling (solid) is larger and less dependent on molecular geometry than either of the individual coupling constants $^3J_{H\alpha H\beta 2}$ (dashed) and $^3J_{H\alpha H\beta 3}$ (dot-dashed). Magnetization transfer, and therefore sensitivity, is most efficient when the target coupling $^3J(H^\alpha,C^\gamma)$ is smallest. Situations are shown for various extents of χ_1-angular mobility according to a Gaussian mode with spread $\pm\sigma$ as indicated.

fully labelled biomolecules often suffers from efficient transverse relaxation governed by dipolar interaction and that higher order multiple-quantum coherence might offer a solution to this drawback. Marino and co-workers (1997) were the first to propose ct-HTQC experiments as CH_2-triple quantum coherence is supposed to decay slower than CH-double quantum coherence. Correspondingly, during the constant-time delay in our ct-HTQC-COSY experiment, the $C^\beta H_2$-triple quantum coherence anti-phase with respect to the H^α spin, $8S_{1x}(I_{1x}^{(1)}I_{1y}^{(2)} + I_{1y}^{(1)}I_{1x}^{(2)})I_{2z}$, experiences fewer relaxation pathways than $C^\beta H$-double quantum coherence anti-phase with respect to both H^α and the partner H^β nuclei, $8S_{1y}(I_{1x}^{(1)}I_{1z}^{(2)} + I_{1z}^{(1)}I_{1x}^{(2)})I_{2z}$, encountered in ct-HMQC-COSY.

As the $H^{\beta 2}$ and $H^{\beta 3}$ spins are mutually exchangeable and magnetization ends up on the H^α spin for either possible transfer, the 2D (C^β,H^α) multiplets obtained are superpositions of two contributions with identical detection frequencies. However, precession frequencies of the H^β spins are not necessarily identical, giving rise to separate 3D multiplets in the indirect dimension F_2. A more elegant approach, which in fact we tried in the first instance, would take advantage of $H^{\beta 2}$,$H^{\beta 3}$ double-quantum precession in order to frequency-encode in the time domain t_2 a combined difference-chemical shift $\omega_{I_1I_1} = \omega_{I_1^{(1)}} + \omega_{I_1^{(2)}} - 2\omega_0$, therefore giving a single multiplet with superior signal-to-noise. This would be achieved using the pulse scheme of Figure 1a by incremental moves of the central proton-refocussing pulse in either direction towards one of the flanking DEPT modules. In practice, the method was successful and has been applied to the flavodoxin sample. However, the 3D lineshape obtained showed twists due to combined absorptive and dispersive components resisting correction to pure phase (Norwood, 1992). The principal difficulty was recognised to be the generation of terms like $2S_{1x}\{2QC\}_x = 4S_{1x}(I_{1x}^{(1)}I_{1x}^{(2)} - I_{1y}^{(1)}I_{1y}^{(2)})$, critically required for pure-phase acquisition. The remedy

was to insert a pair of 180°-refocussing pulses into the first DEPT module as depicted in the pulse scheme of Figure 1b.

Conclusions

The use of CH_2-triple quantum directed coherence filtering enabled otherwise hardly accessible side-chain related $^3J(H^\alpha,C^\gamma)$ coupling constants to be measured in aspartate, asparagine, and aromatic residues in polypeptides. The particular advantage of the new pulse sequence over previous heteronuclear relayed E.COSY schemes is that, rather than a single proton, two geminal spins in a methylene group are exploited for rapid relayed magnetization transfer. The weakest signal intensities are expected in situations when both $^3J(H^\alpha,H^\beta)$ couplings are small owing to a *gauche–gauche* (g^2g^3) arrangement, i.e. when $\chi_1 \approx +60°$, in which case, however, the target $^3J(H^\alpha,C^\gamma)$ coupling constant is at its maximum. For all the other rotational states encountered in these amino acids, COSY-type magnetization transfer is highly efficient because the indiscriminate sum of the coupling constants $^3J(H^\alpha,H^{\beta2})$ and $^3J(H^\alpha,H^{\beta3})$ comfortably exceeds 10 Hz (Figure 4). Irrespective of the underlying molecular geometry, a composite $^3J(H^\alpha,H^\beta)$ coupling of 17 Hz would optimally match the fixed period for magnetization transfer T, as determined by the refocusing of the $^1J(C^\alpha,C^\beta)$ coupling in the present application. Last but not least, the correspondingly large antiphase splitting along the detection dimension of the multiplet is less prone to line cancellation.

Acknowledgements

Dr. Geoff Kelly is thanked for critical reading of the manuscript and for helpful discussion. C.P. acknowledges a grant from the Deutscher Akademischer Austauschdienst (DAAD). This work was supported by the Deutsche Forschungsgemeinschaft under grant Schm 854/4-1.

References

Aue, W.P., Bartholdi, E. and Ernst, R.R. (1976) *J. Chem. Phys.*, **64**, 2229–2246.

Bax, A., Vuister, G.W., Grzesiek, S., Delaglio, F., Wang, A.C., Tschudin, R. and Zhu, G. (1994) *Methods Enzymol.*, **239**, 79–105.

Blümel, M., Schmidt, J.M., Löhr, F. and Rüterjans, H. (1998) *Eur. Biophys. J.*, **27**, 321–334.

DeMarco, A., Llinás, M. and Wüthrich, K. (1978) *Biopolymers*, **17**, 617–636.

DeMarco, A. and Llinás, M. (1979) *Biochemistry*, **18**, 3846–3854.

Eggenberger, U., Schmidt, P., Sattler, M., Glaser, S.J. and Griesinger, C. (1992) *J. Magn. Reson.*, **100**, 604–610.

Emsley, L. and Bodenhausen, G. (1990) *Chem. Phys. Lett.*, **165**, 469–476.

Ernst, R.R., Bodenhausen, G. and Wokaun, A. (1987) *Principles of Nuclear Magnetic Resonance in One and Two Dimensions*, Clarendon Press, Oxford, U.K.

Griesinger, C., Sørensen, O.W. and Ernst, R.R. (1986) *J. Chem. Phys.*, **85**, 6837–6852.

Griffey, R.H. and Redfield, A.G. (1987) *Quart. Rev. Biophys.*, **19**, 51–82.

Grzesiek, S. and Bax, A. (1993) *J. Biomol. NMR*, **3**, 185–204.

Grzesiek, S. and Bax, A. (1995) *J. Biomol. NMR*, **6**, 335–339.

Gschwind, R.M., Gemmecker, G. and Kessler, H. (1998) *J. Biomol. NMR*, **11**, 191–198.

Karimi-Nejad, Y. (1994) Thesis, University of Cologne, Germany.

Logan, T.M., Olejniczak, E.T., Xu, R.X. and Fesik, S.W. (1992) *FEBS Lett.*, **314**, 413–418.

Löhr, F., Blümel, M., Schmidt, J.M. and Rüterjans, H. (1997) *J. Biomol. NMR*, **10**, 107–118.

Löhr, F. and Rüterjans, H. (1995) *J. Biomol. NMR*, **5**, 25–36.

Löhr, F. and Rüterjans, H. (1999) *J. Biomol. NMR*, **13**, 263–274.

Marino, J.P., Diener, J.L., Moore, P.B. and Griesinger, C. (1997) *J. Am. Chem. Soc.*, **85**, 2870–2871.

Marion, D., Ikura, M., Tschudin, R. and Bax, A. (1989) *J. Magn. Reson.*, **85**, 393–399.

Martinez-Oyanedel, J., Choe, H.W., Heinemann, U. and Saenger, W. (1991) *J. Mol. Biol.*, **222**, 335–352.

Mattiello, D.L., Warren, W.S., Mueller, L. and Farmer II, B.T. (1996) *J. Am. Chem. Soc.*, **118**, 3253–3261.

Norwood, T.J. (1992) *Prog. NMR Spectrosc.*, **24**, 295–375.

Piantini, U., Sørensen, O.W. and Ernst, R.R. (1982) *J. Am. Chem. Soc.*, **104**, 6800–6801.

Schmidt, J.M. (1997) *J. Magn. Reson.*, **124**, 298–309.

Schmidt, J.M., Blümel, M., Löhr, F. and Rüterjans, H. (1999) *J. Biomol. NMR*, **14**, 1–12.

Schmidt, J.M., Ernst, R.R., Aimoto, S. and Kainosho, M. (1995) *J. Biomol. NMR*, **6**, 95–105.

Schmidt, J.M., Löhr, F. and Rüterjans, H. (1996) *J. Biomol. NMR*, **7**, 142–152.

Schmidt, J.M. and Rüterjans, H. (1990) *J. Am. Chem. Soc.*, **112**, 1279–1280.

Seip, S., Balbach, J. and Kessler, H. (1992) *J. Magn. Reson.*, **100**, 406–410.

Shaka, A.J., Barker, P.B. and Freeman, R. (1985) *J. Magn. Reson.*, **64**, 547–552.

Sklenár, V., Dieckmann, T., Butcher, S.E. and Feigon, J. (1998) *J. Magn. Reson.*, **130**, 119–124.

Smallcombe, S.H., Patt, S.L. and Keifer, P.A. (1995) *J. Magn. Reson.*, **A117**, 295–303.

Swapna, G.V.T., Rios, C.B., Shang, Z. and Montelione, G.T. (1997) *J. Biomol. NMR*, **9**, 105–111.

Tessari, M., Gentile, L.N., Taylor, S.J., Shalloway, D.I., Nicholson, L.K. and Vuister, G.W. (1997) *Biochemistry*, **36**, 14561–14571.

Vuister, G.W. and Bax, A. (1993) *J. Magn. Reson.*, **B102**, 228–231.

Wasylishen, R. and Schaefer, T. (1972) *Can. J. Chem.*, **50**, 2710–2712.

Watt, W., Tulinsky, A., Swenson, R.P. and Watenpaugh, K.D. (1991) *J. Mol. Biol.*, **218**, 195–208.